Cell Reports, Volume *16*

Supplemental Information

MICU1 Serves as a Molecular Gatekeeper to Prevent In Vivo Mitochondrial Calcium Overload

Julia C. Liu, Jie Liu, Kira M. Holmström, Sara Menazza, Randi J. Parks, Maria M. Fergusson, Zu-Xi Yu, Danielle A. Springer, Charles Halsey, Chengyu Liu, Elizabeth Murphy, and Toren Finkel

Fig. S1, related to Fig. 1

A

```
                                        MICU1-sgRNA 1
MICU1 WT:    TCATTTGTCCACAGGATGTTTCGTCTTAACACCCTTTCTGCGTTGGCAGAACTAGCTGTGGGCTCTCGCTGGTACCATGGGGCATC
MICU1 KO-1:  TCATTTGTCC----------------ACACCCTTTCTGCGTTGGCAGAACTAGCTGTGGGCTCTCGCTGGTACCATGGGGCATC
MICU1 KO-2:  TCATTTGTCCACAGGATGTTTCGTCTTAACACCCTTTCTGCGTTGGCAGAACTAGCTGTGGGCTCTCGCTGGTACCATGGGG----
MICU1 KO-3:  TCATTTGTCCACAGGATGTTTCGTCTTAACACCCTTTCTGCGTTGGCAGAACTAGCTGTGGGCTCTCGCTGGTACCATGGGGCATC
MICU1 KO-4:  TCATTTGTCCACAGGATGTTTCGTCTTAACACCCTTTCTGC----------------------------------------

                                                                                MICU1-sgRNA 2
MICU1 WT:    ACAGCCCACACAGACCAAACGAAGATTGATGCTGGTGGCGTTCCTGGGAGCATCTGCAGTGACTGCAAGTACCGGTCTCCTGTGGA
MICU1 KO-1:  ACAGCCCACACAGACCAAACGAAGATTGATGCTGGTGGCGTTCCTGGGAGCATCTGCAGTGACTGCAAGTACCGGTCTCCTGTGGA
MICU1 KO-2:  ------------------------------------------------------------------------TACCGGTCTCCTGTGGA
MICU1 KO-3:  ACAGCCCACACAGACCAAACGAAGATTGATGCTGGTGGCGTTCCTGGGAGCATCTGCAGTGA----------------------
MICU1 KO-4:  ------------------------------------------------------------------------TACCGGTCTCCTGTGGA

MICU1 WT:    AGAAGTGAGTGTTATTTCAGGCTTGCTTTTACATCAGAATTTCTTTGCTGAATTG
MICU1 KO-1:  AGAAGTGAGTGTTATTTCAGGCTTGCTTTTACATCAGAATTTCTTTGCTGAATTG
MICU1 KO-2:  AGAAGTGAGTGTTATTTCAGGCTTGCTTTTACATCAGAATTTCTTTGCTGAATTG
MICU1 KO-3:  --------------------------------TCAGAATTTCTTTGCTGAATTG
MICU1 KO-4:  AGAAGTGAGTGTTATTTCAGGCTTGCTTTTACATCAGAATTTCTTTGCTGAATTG
```

B

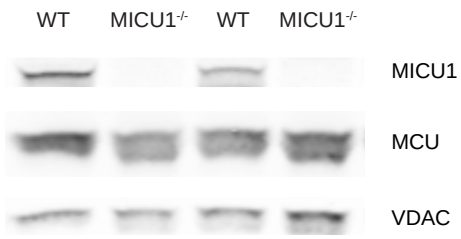

C

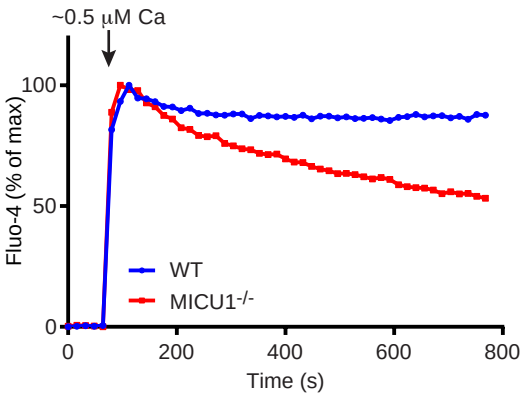

D

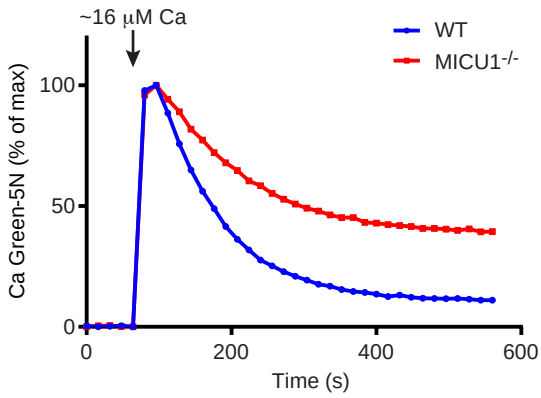

Fig. S2, related to Fig. 2

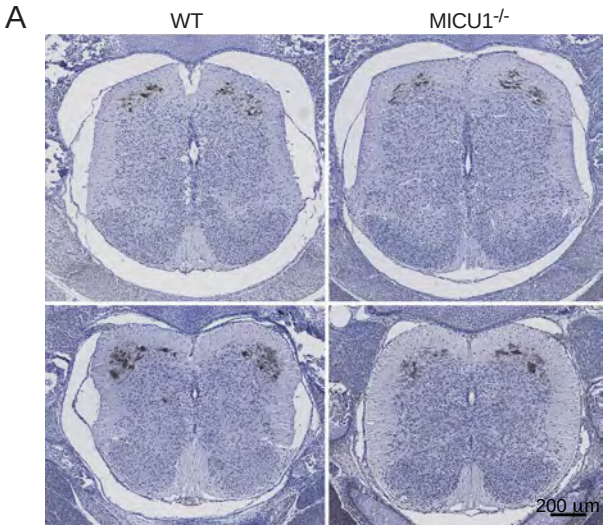

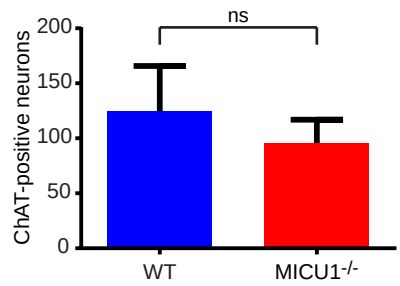

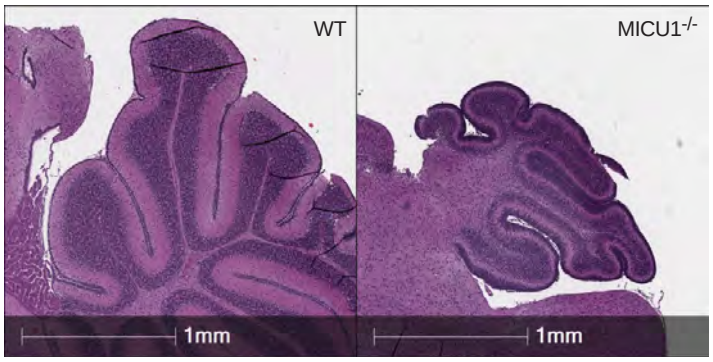

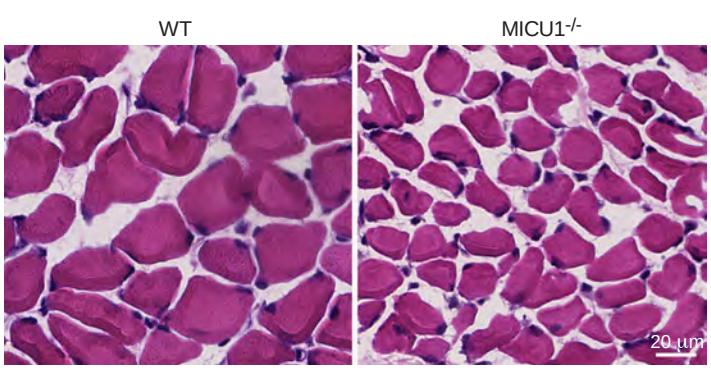

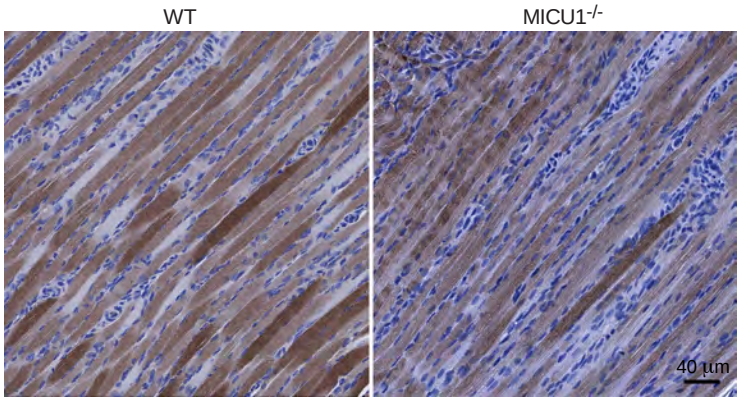

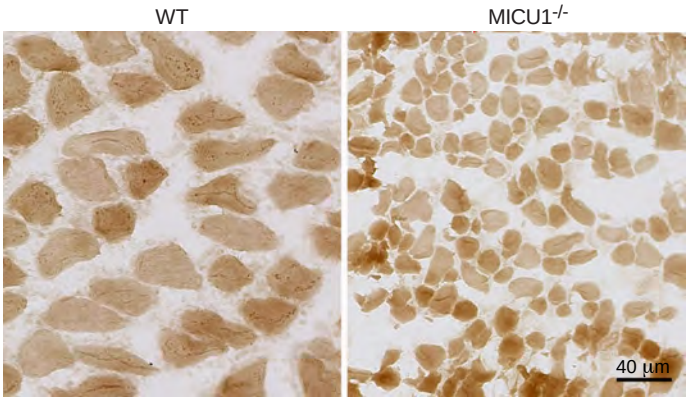

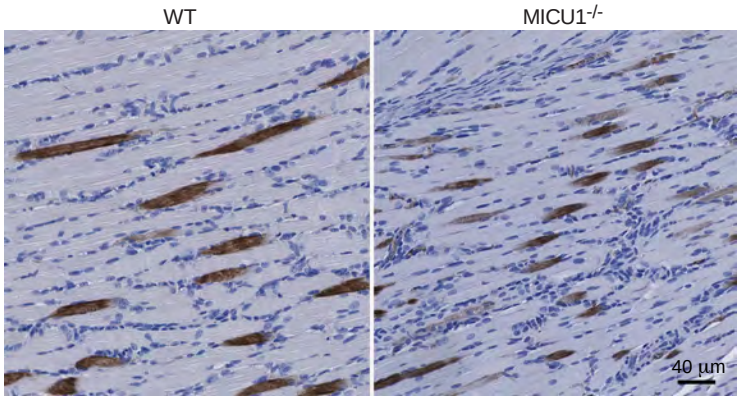

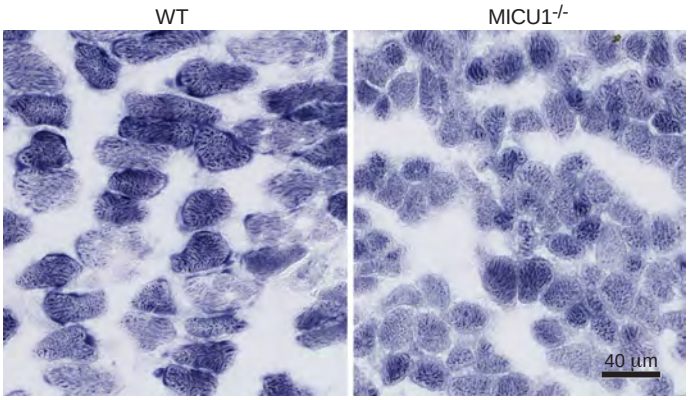

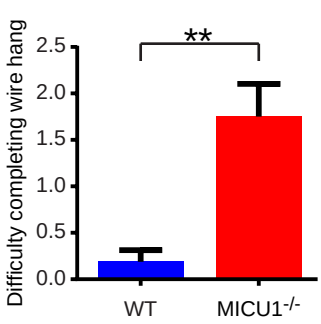

Fig. S3, related to Fig. 2

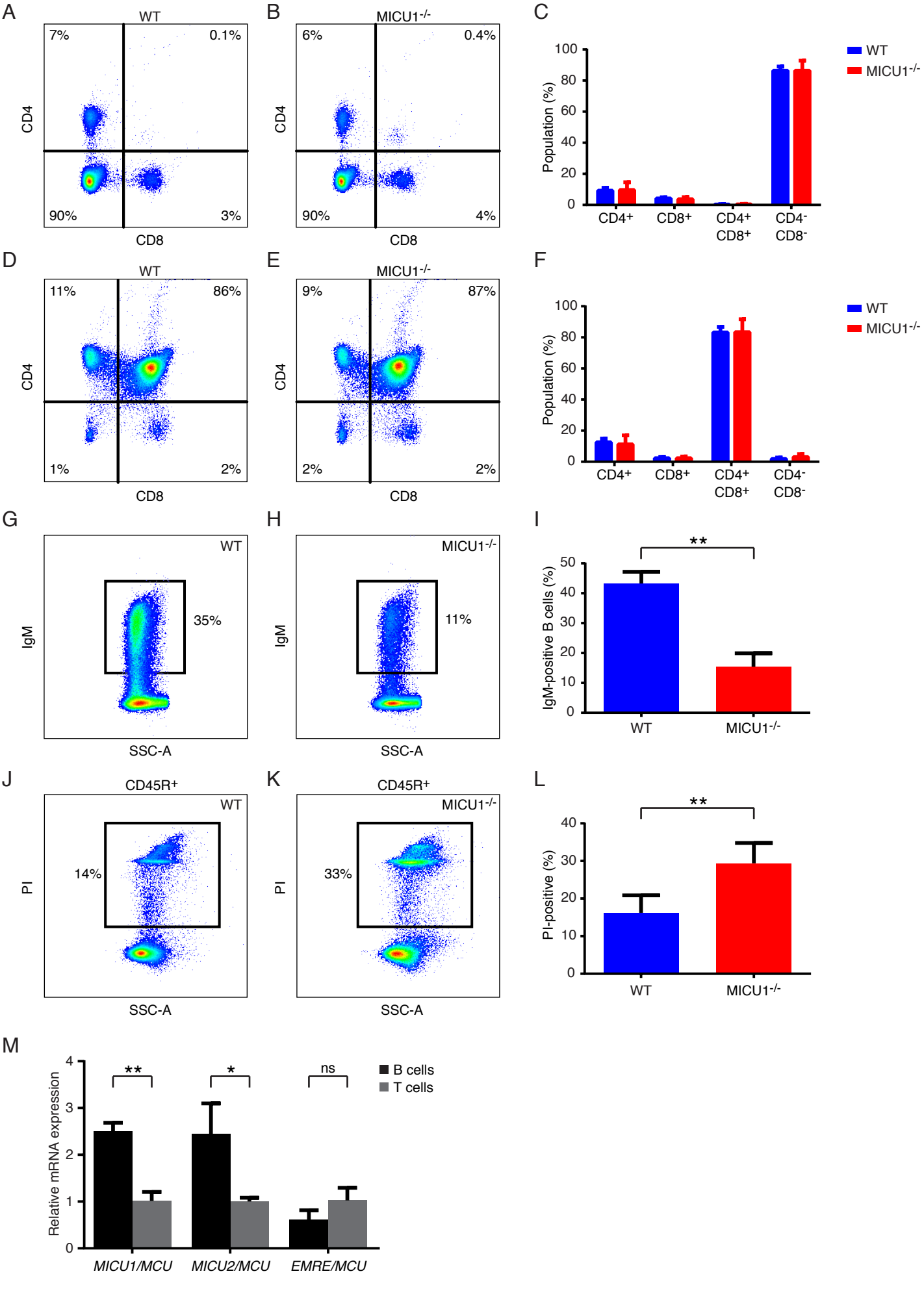

Fig. S4, related to Fig. 3

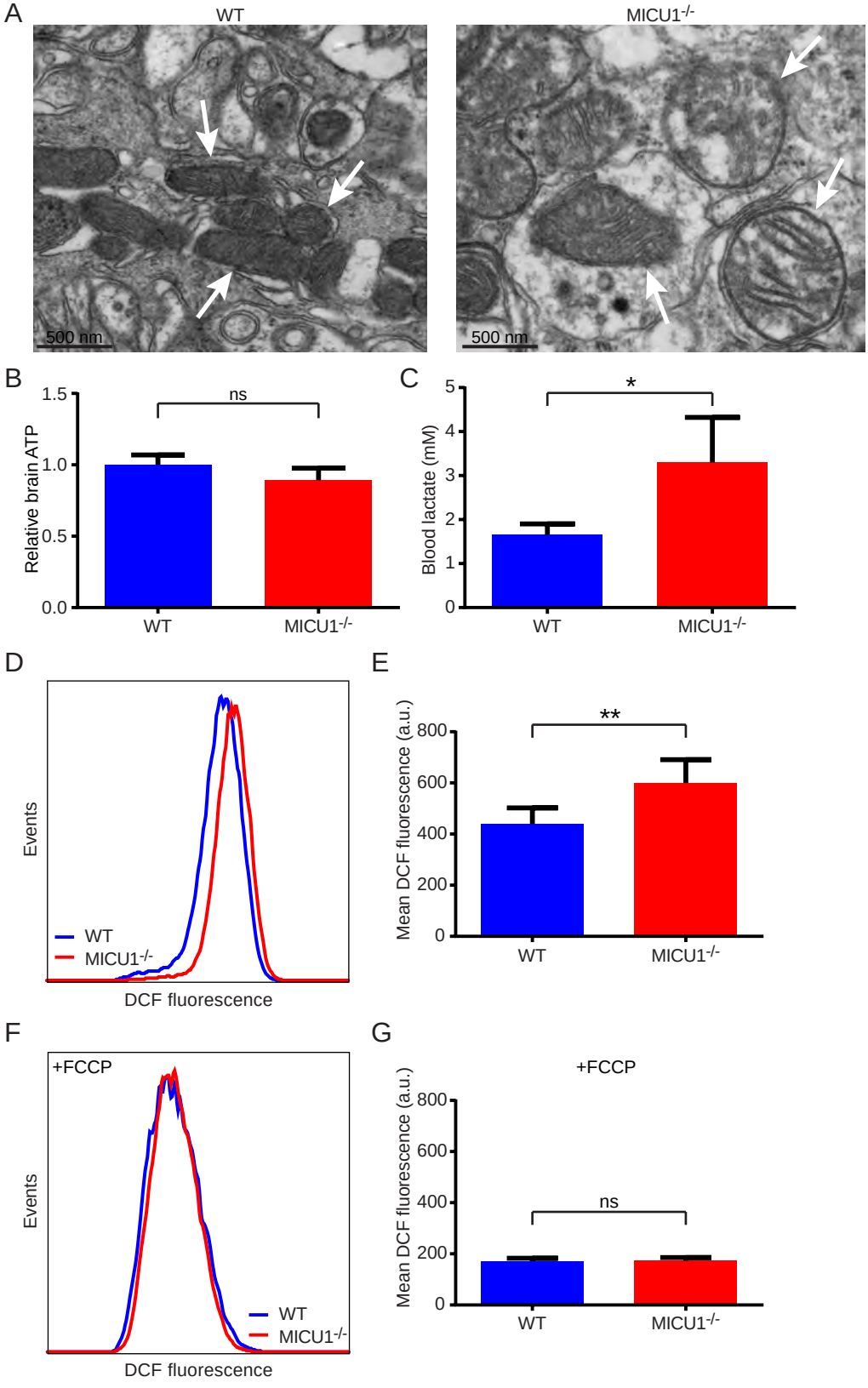

Fig. S5, related to Fig. 4

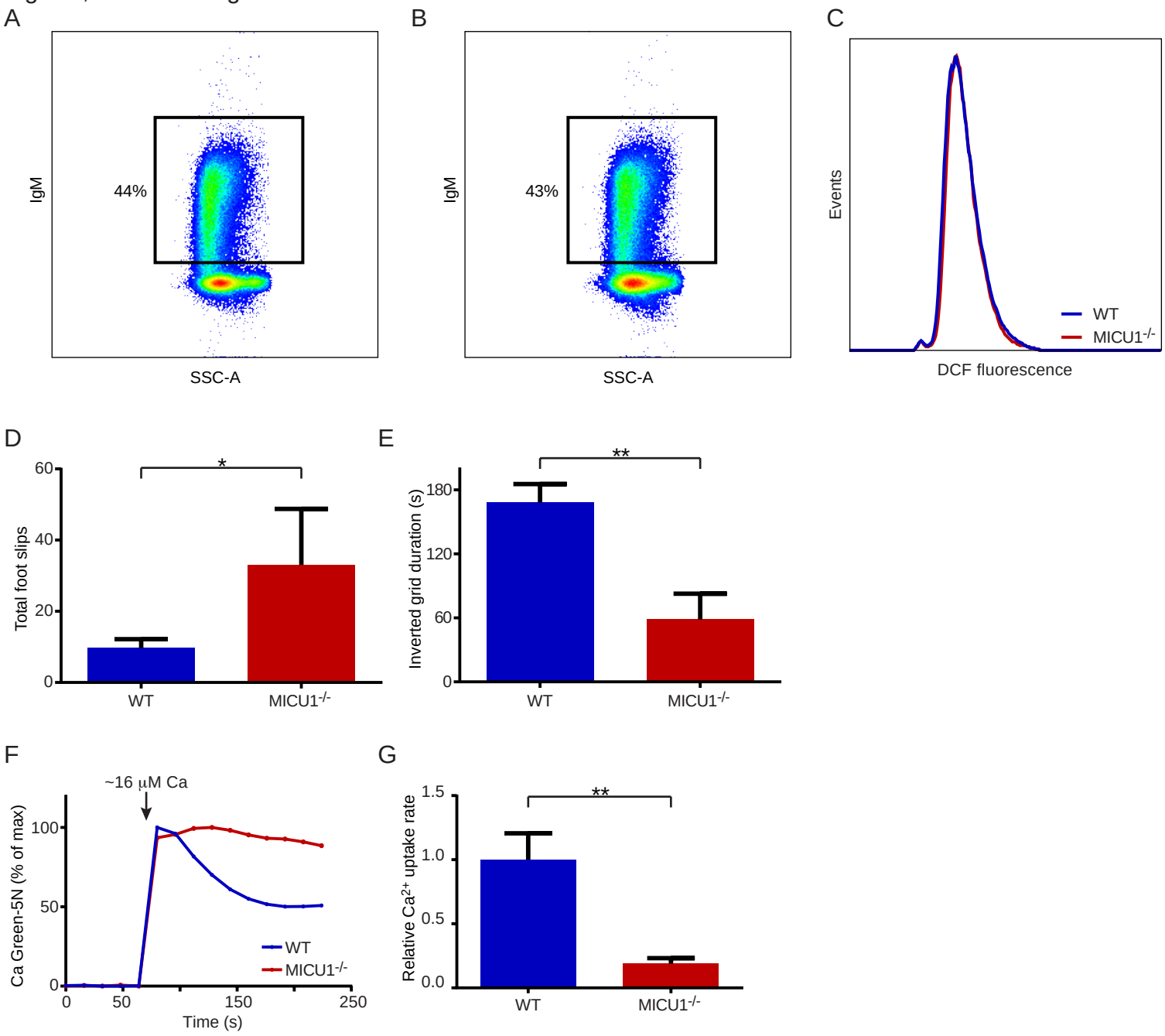

Fig. S6, related to Fig. 6

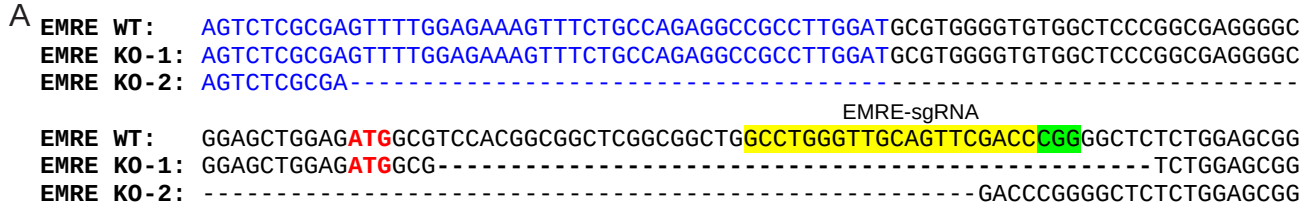

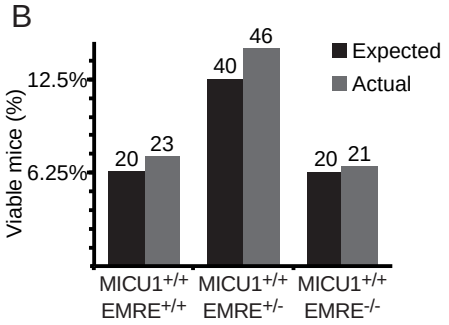

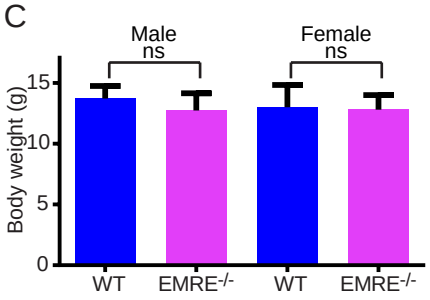

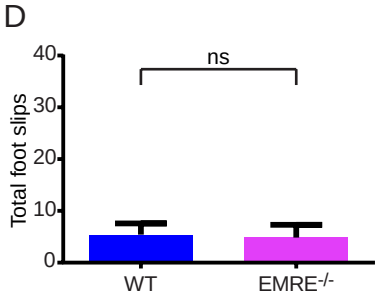

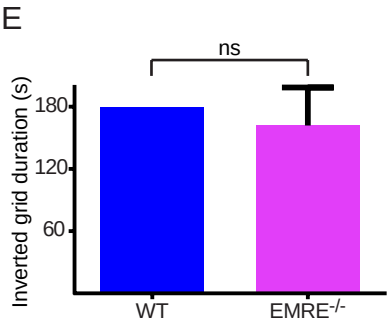

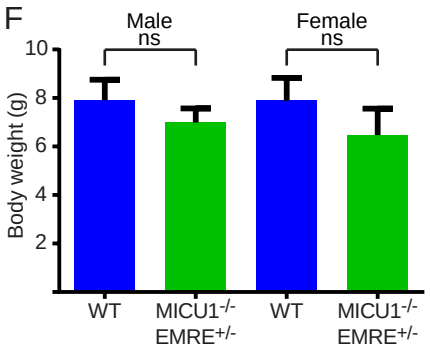

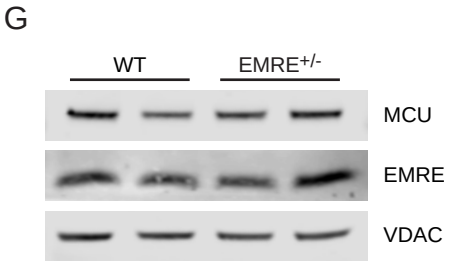

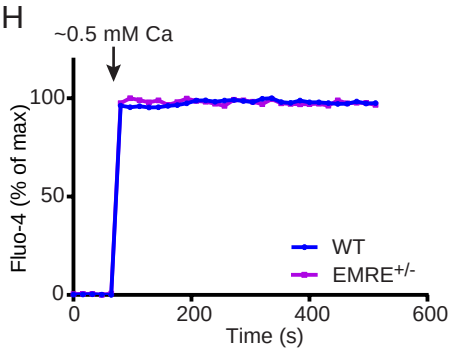

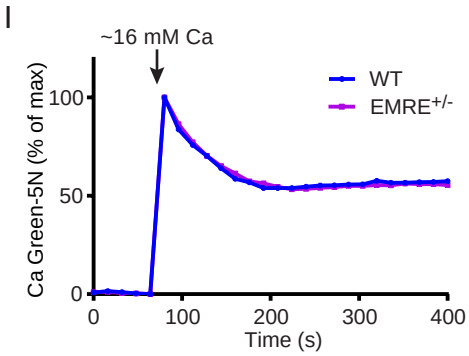

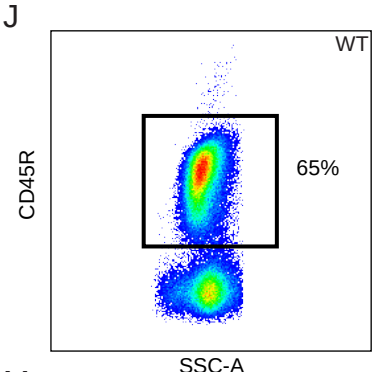

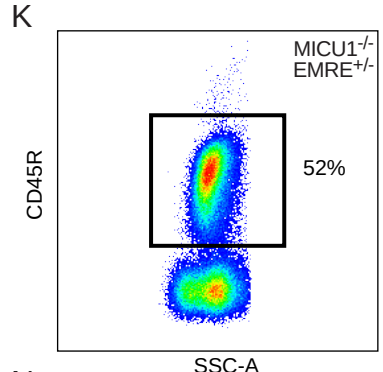

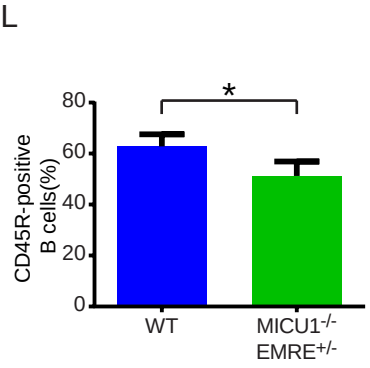

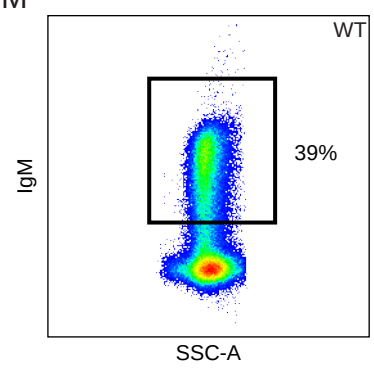

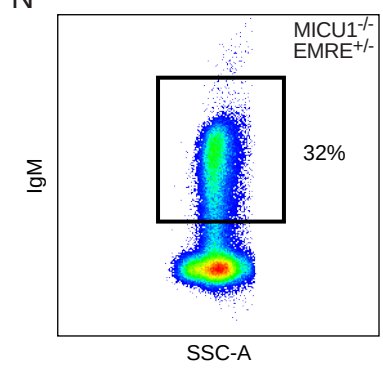

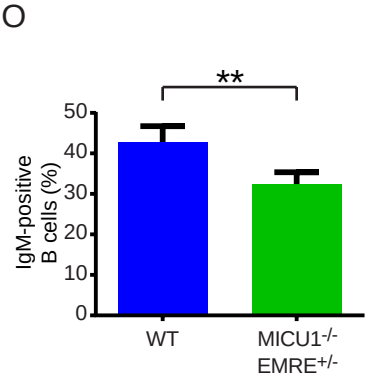

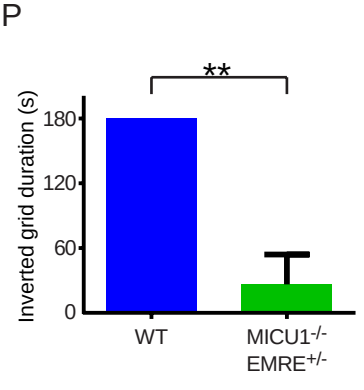

Supplemental Figure Legends:

Figure S1: Generation of MICU1 knockout mice. **A**) CRISPR-mediated deletions in various MICU1 knockout mouse lines. The sequence of MICU1 exon 2 (first coding exon) is shown in black and intron 2 is depicted in blue. The two CRISPR binding sites are highlighted in yellow, and their PAMs are highlighted in green. The translational initiation codon (ATG) is shown in red. In the MICU1 KO-4 mouse line, there is a 114 bp deletion, but the five underlined nucleotides (CGGTC) were duplicated. **B)** Western blot of MICU1 and MCU levels in liver mitochondria obtained from WT and MICU1$^{-/-}$ mice. The mitochondrial protein VDAC is shown as a loading control. **C**) Representative extra-mitochondrial calcium traces with WT or MICU1$^{-/-}$ brain mitochondria using the calcium indicator Fluo-4. Estimated free calcium concentration is 0.5 µM. **D**) Representative extra-mitochondrial calcium traces with WT or MICU1$^{-/-}$ brain mitochondria at high free calcium concentration (estimated at 16 µM) using Calcium Green-5N as an indicator.

Figure S2: Phenotypic assessment of MICU1$^{-/-}$ mice. **A**) Representative images of anti-choline acetyltransferase (ChAT) labeling of cervical motor neurons in two pairs of WT and MICU1$^{-/-}$ mice that are approximately at E19. **B**) Quantification of the number of ChAT-positive cervical motor neurons in WT and MICU1$^{-/-}$ mice (n=3 WT, n=5 MICU1$^{-/-}$). Data are represented as mean ± SD. **C**) Cerebellar architecture of WT and MICU1$^{-/-}$ mice at 12 days of age. **D**) Quadriceps muscle fiber architecture of WT and MICU1$^{-/-}$ mice demonstrating the absence of central nuclei in MICU1$^{-/-}$ muscle. **E**) Representative staining of fast muscle fibers in gastrocnemius muscle from WT and MICU1$^{-/-}$ mice. **F**) Representative staining of slow muscle fibers in gastrocnemius muscle from WT and MICU1$^{-/-}$ mice. **G**) Concurrent staining of cytochrome c oxidase (COX) and succinate dehydrogenase (SDH) activity in cryosections of WT and MICU1$^{-/-}$ quadriceps muscle. Brown staining reflects muscle COX activity. **H**) As a control, SDH activity (blue staining) alone was assessed in cryosections. **I**) Wire hang test for WT and MICU1$^{-/-}$ mice. In this exam, which requires the mouse to pull up on a wire and subsequently get its hind limbs over the wire, a low score denotes higher function (n=4 per genotype, mean ± SD). **p<0.01, *p<0.05

Figure S3: Phenotypic assessment of MICU1$^{-/-}$ B cells and T cells. **A**) Representative level of splenic T cell maturation as assessed by surface CD4^{+} or CD8^{+} markers in WT or **B**) MICU1$^{-/-}$ mice. **C**) Quantification of splenic T cell maturation (n=5 per genotype, data are represented as mean ± SD; p = NS for all comparisons between WT and MICU1$^{-/-}$ cells). **D**) Representative level of thymic T cell maturation as assessed by surface CD4^{+} or CD8^{+} markers in WT or **E**) MICU1$^{-/-}$ mice. **F**) Quantification of thymic T cell maturation (n=8 WT and n=7 MICU1$^{-/-}$, mean ± SD; p = NS for all comparisons between WT and MICU1$^{-/-}$ cells). **G**) Representative level of mature IgM-positive B cells in the spleen of WT or **H**) MICU1$^{-/-}$ mice. **I**) Quantification of splenic IgM-positive B cells in WT and MICU1$^{-/-}$ mice (n=6 per genotype, mean ± SD). **J**) Representative percentage of CD45R-positive splenic B cells which are non-viable as assessed by positive staining for propidium iodide (PI) in WT or **K**) MICU1$^{-/-}$ mice. **L**) Levels of PI-positive, CD45R-positive splenic B cells in WT or MICU1$^{-/-}$ mice (n=6 per genotype, mean ± SD). **M**) Relative mRNA expression of uniporter components in WT B cells and T cells. Values are expressed relative to MCU and normalized to the ratio observed in T cells (n=4 WT mice per group). **p<0.01, *p<0.05

Figure S4: MICU1$^{-/-}$ mice exhibit mitochondrial defects. **A**) Electron micrograph of WT and MICU1$^{-/-}$ cerebellum at 5 weeks of age. Arrows indicate mitochondria. **B**) Relative ATP levels in the cerebellum of 5-week-old WT and MICU1$^{-/-}$ mice (n=3 per genotype, data are represented as mean ± SD). **C**) Blood lactate levels in 6-week-old WT and MICU1$^{-/-}$ mice (n=4 per genotype, mean ± SD). **D**) Representative DCFDA staining of thymus-derived T cells obtained from WT and MICU1$^{-/-}$ mice. **E**) Quantification of mean DCF fluorescent intensity expressed in arbitrary units (a.u.) using T cells obtained from WT and MICU1$^{-/-}$ mice (n=8 per genotype, mean ± SD). **F**) Representative DCFDA staining of thymus-derived T cells obtained from WT and MICU1$^{-/-}$ mice 30 minutes after treatment with the mitochondrial uncoupling agent FCCP (5 μM). **G**) Quantification of mean DCF fluorescent intensity (arbitrary units) from T cells obtained from WT and MICU1$^{-/-}$ mice in the presence of the mitochondrial uncoupling agent FCCP (n=3 per genotype, mean ± SD; p = NS). **p<0.01, *p<0.05

Figure S5: Phenotypic assessment of older MICU1$^{-/-}$ mice. **A**) Representative level of mature IgM-positive B cells in the spleen of 7-month-old WT or **B**) MICU1$^{-/-}$ mice. **C**) Representative DCFDA staining of thymus-derived T cells obtained from 7-month-old WT and MICU1$^{-/-}$ mice. **D**) Cerebellar function in 4-month-old WT and MICU1$^{-/-}$ mice assessed by performance on a balance beam and measured as cumulative number of foot slips (n=6 per genotype, data are represented as mean ± SD). **E**) Assessment of muscle strength in WT and MICU1$^{-/-}$ mice using an inverted grid test at 4 months of age (n=6 mice per genotype, mean ± SD). **F**) Representative extra-mitochondrial calcium traces with WT or MICU1$^{-/-}$ liver mitochondria from 7-month-old mice at high free calcium concentration (estimated at 16 μM) using Calcium Green-5N as an indicator. **G**) Quantification of calcium uptake rates in liver mitochondria from 7-month-old mice at high (16 μM) extra-mitochondrial free calcium concentration (n=3 per genotype, mean ± SD).

Figure S6: EMRE heterozygosity rescues MICU1 deletion. **A**) CRISPR-mediated deletions in two EMRE knockout mouse lines. The sequence of EMRE exon 1 is shown in black and the upstream noncoding region is depicted in blue. The CRISPR binding site is highlighted in yellow, and its PAM is highlighted in green. The translational initiation codon (ATG) is shown in red. Two independent lines were generated, and both lines when bred to MICU1$^{-/-}$ mice were able to produce MICU1$^{-/-}$EMRE$^{+/-}$ offspring. **B**) Percentage of observed and expected MICU1$^{+/+}$ mice surviving past one week with either EMRE$^{+/+}$, EMRE$^{+/-}$, and EMRE$^{-/-}$ genotype status. Actual number of expected and observed mice from MICU1$^{+/-}$EMRE$^{+/-}$ crosses is shown above each bar. **C**) Weights of male (n=5 WT, n=4 EMRE$^{-/-}$) and female (n=4 WT, n=4 EMRE$^{-/-}$) mice at 3 weeks of age (mean ± SD). All data on EMRE$^{-/-}$ mice were generated from one mouse line (EMRE KO-1 in Figure S6A) in a mixed genetic background. **D**) Cerebellar function in 4-week-old WT and EMRE$^{-/-}$ mice assessed by performance on a balance beam and measured as cumulative number of foot slips (n=5 WT, n=6 EMRE$^{-/-}$, data are represented as mean ± SD). **E**) Assessment of muscle strength in 4-week-old WT and EMRE$^{-/-}$ mice using an inverted grid test (n=5 mice per genotype, mean ± SD). **F**) Weights of male (n=4 WT, n=5 MICU1$^{-/-}$EMRE$^{+/-}$) and female (n=5 WT, n=5 MICU1$^{-/-}$EMRE$^{+/-}$) mice at 14-18 days of age. **G**) Western blot of MCU and EMRE expression in liver mitochondria from WT and EMRE$^{+/-}$ mice. **H**) Representative calcium uptake of WT and EMRE$^{+/-}$ liver mitochondria under low calcium conditions or **I**) at high calcium concentrations. **J**) Representative level of CD45R-positive B cells in spleens of WT or **K**) MICU1$^{-/-}$EMRE$^{+/-}$ mice. **L**) Mean B cell percentage as assessed by CD45R staining in

spleens of WT (n=6) and MICU1$^{-/-}$EMRE$^{+/-}$ (n=3) mice (mean ± SD). **M**) Representative level of mature IgM-positive B cells in spleens of WT or **N**) MICU1$^{-/-}$EMRE$^{+/-}$ mice. **O**) Mean B cell percentage as assessed by IgM staining in spleens of WT (n=6) and MICU1$^{-/-}$EMRE$^{+/-}$ (n=3) mice (mean ± SD). **P**) Assessment of skeletal muscle strength using an inverted grid test in 4-week-old WT (n=5) and MICU1$^{-/-}$EMRE$^{+/-}$ (n=10) mice (mean ± SD). **p<0.01, *p<0.05

Supplemental Movie 1. A freely behaving one-year-old female MICU1$^{-/-}$ mouse exhibiting chorea-like movements.

Supplemental Experimental Procedures:

Western blot

For western blot analysis, mitochondria were isolated as described above. MEFs were solubilized in cell lysis buffer (Cell Signaling) in the presence of protease inhibitors (Roche). Protein content was measured using the BCA assay (Thermo Scientific) and samples were diluted in SDS-sample buffer (Boston BioProducts), heated to 37°C for 10 min prior to SDS-PAGE. Following transfer to nitrocellulose, membranes were immunoblotted with primary antibodies against MICU1 (Sigma HPA037480), MCU (Sigma HPA016480), EMRE (Santa Cruz Biotechnology sc-86337), VDAC (Abcam ab154856), COX4 / Complex IV Subunit IV (Life Technologies A21348), and beta-tubulin (Developmental Studies Hybridoma Bank E7). Proteins were visualized using LI-COR secondary antibodies and the Odyssey imaging system.

ATP and lactate assay

Extraction of ATP from skeletal muscle (50-60 mg per sample) was performed using the phenol-TE method (Chida et al., 2012). ATP levels were then determined using the Luminescent ATP Detection Assay Kit (Abcam) according to the manufacturer's instructions and normalized to the initial weight of the tissue. Relative ATP concentrations were normalized to WT levels. Lactate levels were measured in skeletal muscle using ThermoFisher Trace GC Ultra/DSQ II single quadrupole mass spectrometer and standard GC/MS methods as previously described (Pan et al., 2013). Blood lactate levels were measured from mouse tail vein using a lactate meter (Nova Biomedical).

Flow cytometry and qPCR

Mouse thymocytes and splenocytes were immunophenotyped using the following antibodies: CD4-APC (clone RM4-5), CD8a-APC-CY7 (clone 53-6.7), CD45R-APC (clone RA3-6B2), and IgM-APC (all from BD Pharmingen). For assessment of ROS levels in B cells and thymocytes, we loaded cells with the redox-sensitive fluorophore 2',7' –dichlorofluorescin diacetate DCFDA (5 μM, Molecular Probes) as we have previously described (Liu et al., 2009). Where indicated, cells were treated with the mitochondrial uncoupling agent carbonyl cyanide-4-(trifluoromethoxy)phenylhydrazone (FCCP; 5 μM) for 30 min at

37°C prior to analysis. Dead cells were gated by propidium iodide staining. Flow cytometry was performed on a BD FACS Canto (BD Biosciences) and analysis was done in FlowJo.

RNA was extracted from B cells and T cells using TRIzol reagent (Life Technologies) according to manufacturer's instructions. RNA was reverse transcribed using the iScript cDNA Synthesis Kit (Bio-Rad) and quantitative real-time PCR was performed on a MxP3005P real-time PCR system (Stratagene) using FastStart Universal Probe Master (Roche) according to manufacturer's instructions. The following primer sequences were used: MCU, forward primer: 5'-GTGCCCTCTGATGACGTGACGG-3', reverse primer: 5'-ATGACAAGCTTAAAGTCATC-3'; MICU1, forward primer: 5'-ACACCCTCAAGTCTGGCTTAT-3', reverse primer: 5'-TTCCCATCTTTGAAGTGCTTCTT-3'; MICU2, forward primer: 5'-TCGGCGCAGAAAAATTATTTGG-3', reverse primer: 5'-GTGTCATGTAATACTCTCCGTCG-3'; EMRE, forward primer: 5'-CATTTTGCCCAAGCCGGTG-3', reverse primer: 5'- CCTGTGCCCTGTTAATCGTCGT-3'. The following primer sequences were used for reference genes: eukaryotic translation initiation factor EIF35S, forward primer: 5'-CTGAGGATGTGCTGTCTGGGAA-3', reverse primer: 5'-CCTTTGCCTCCACTTCGGTC-3'; ribosomal protein 36B4, forward primer: 5'- TGAAGTGCTCGACATCACAGA-3', reverse primer: 5'-CACAGACAATGCCAGGACGC-3'; and beta-actin, forward primer: 5'- CCCCTGAGGAGCACCCTG-3', reverse primer: 5'- GACCAGAGGCATACAGGGAC-3'.

Histology

Tissues were fixed in 10% formalin, after which they were embedded in paraffin and sectioned at 5 µm. The sections were stained with H&E using standard methods. For antibody staining, sections were deparaffinnized and unmasked with citrate buffer. After blocking, sections were incubated overnight at 4°C with primary antibodies against calbindin (Sigma C9848), anti-choline acetyltransferase (ChAT) (AB144P, Millipore), myosin heavy chain type I (slow) (NCL-MHCs, Leica Biosystems), myosin heavy chain type II (both IIa and IIb, fast) (NCL-MHCf, Leica Biosystems) . Following washes and incubation with biotinylated secondary antibody, slides were stained with the VECTASTAIN ABC Kit (Vector Laboratories) according to the manufacturer's instructions. Sections were imaged using the NanoZoomer 2.0 (Hamamatsu).

For motor neuron quantification, ChAT-positive motor neurons were counted in the cervical spinal cord from E18 to E20 embryos at levels C3-C5 (every third section; total of four cervical cord sections per mouse).

COX/SDH double-labeling

Cytochrome c oxidase (COX) and succinate dehydrogenase (SDH) double-labeling histochemistry was performed using standard methods (Ross, 2011). In brief, mouse quadricep muscle was frozen in Tissue-Tek O.C.T. compound on dry ice and 10 µm cryostat sections were prepared. For COX staining, thawed samples were incubated in PBS buffer with DAB, cytochrome c, and catalase for 40 min at 37 °C, and then washed 4 times with PBS. Subsequently, samples were incubated in PBS buffer with nitroblue tetrazolium (NBT) and 130 mM sodium succinate for 40 min at 37 °C to stain for SDH activity. SDH staining was also performed without COX staining as a control. After PBS washes, slides were

dehydrated in a range of ethanol solutions, followed by xylene. Coverslips were mounted with Permount and imaged using the NanoZoomer 2.0 (Hamamatsu).

Electron microscopy

Skeletal muscle from mouse thigh and mouse cerebellum were cut with a razor blade into approximately 1 mm^3 cubes and fixed in 2.5% glutaraldehyde and 1% paraformaldehyde in 0.12 M sodium cacodylate buffer, pH 7.4. After fixation, the tissue pieces were postfixed with 1% osmium tetroxide in cacodylate buffer, *en bloc* stained with 1% uranyl acetate, and dehydrated with an ethanol series and propylene oxide. The samples were then embedded in EMbed 812 resin (Electron Microscopy Sciences, Hatfield PA). Ultrathin resin sections were cut and stained with uranyl acetate and lead citrate. Images were acquired on a JEM 1400 electron microscope (JEOL USA, Peabody MA) with an AMT XR-111 digital camera (Advanced Microscopy Techniques Corporation, Woburn MA).

Balance beam, inverted grid, and wire hang tests

Mice were first trained to cross a 32-mm-wide, 80-cm-long beam elevated 50 cm off the floor into an opaque shelter placed at the end of the beam. Twenty-four hours after acclimation and training, the mice were tested using three beams with widths of 24mm, 12mm, and 9mm. Mice received three trials per beam, with a brief rest between trials. Testing started with the least challenging beam width and progressed to the most challenging/narrow beam, with a rest period of one hour between beams. The number of hind and fore limb foot slips and number of falls were recorded. The cumulative number of all foot slips on all three balance beams were tabulated for each mouse, with a fore limb foot slip or a significant lean counted as two foot slips.

Grip strength and coordination in mice were assessed with a non-invasive inverted grid suspension test. Mice were placed on a grid which was slowly turned over 180 degrees, suspending the mice above a padded surface. Latency to fall was timed, with the maximum for any trial set at 180 seconds. Three trials with rest periods in between were conducted per mouse.

In the wire hang test, mice were also tested for strength and toe dexterity. Mice were placed on a suspended wire hanging by their front paws, and scored for their ability to pull themselves onto the wire with the following rubric:

0. Immediately able to pull up hind limbs and grab wire with hind legs and move to end
1. Able to pull up and grab bar with hind legs in <3 seconds and with minimal effort
2. Struggles to pull up and grab bar with hind limbs, taking >3 seconds, or struggles to pull up and repeatedly loses grip, drops hind limbs, and struggles to pull up again
3. Unable to lift up and grab bar with hind limbs
4. Has difficulty pulling up/grabbing bar with hind limbs and falls within seconds
5. Falls immediately

Each mouse was given a score between 0-5 based on the mean score achieved from all four trials. All phenotyping was done in a blinded fashion, although in some cases, the apparent weight difference between WT and MICU1$^{-/-}$ mice made true blinding problematic.

Statistical analysis

All data were analyzed for statistical significance using GraphPad Prism software. Except where indicated, all data are expressed as mean ± standard deviation (SD). When more than two comparisons were made, data were first analyzed by ANOVA, followed by a t-test with Welch's correction to determine significance for each data set. *$p<0.05$ and **$p<0.01$

Supplemental References

Chida, J., Yamane, K., Takei, T., and Kido, H. (2012). An efficient extraction method for quantitation of adenosine triphosphate in mammalian tissues and cells. Anal Chim Acta *727*, 8-12.

Liu, J., Cao, L., Chen, J., Song, S., Lee, I.H., Quijano, C., Liu, H., Keyvanfar, K., Chen, H., Cao, L.Y.*, et al.* (2009). Bmi1 regulates mitochondrial function and the DNA damage response pathway. Nature *459*, 387-392.

Pan, X., Liu, J., Nguyen, T., Liu, C., Sun, J., Teng, Y., Fergusson, M.M., Rovira, II, Allen, M., Springer, D.A.*, et al.* (2013). The physiological role of mitochondrial calcium revealed by mice lacking the mitochondrial calcium uniporter. Nature cell biology *15*, 1464-1472.

Ross, J.M. (2011). Visualization of mitochondrial respiratory function using cytochrome c oxidase/succinate dehydrogenase (COX/SDH) double-labeling histochemistry. J Vis Exp, e3266.